Recent advances in high-resolution Ground Penetrating Radar on board an Unmanned Aerial Vehicle

Maria Garcia-Fernandez[1], Yuri Alvarez-Lopez[1], Borja Gonzalez-Valdes[2], Yolanda Rodriguez-Vaqueiro[2], Ana Arboleya-Arboleya[3], Fernando Las Heras[1]

[1](Affiliation): Area of Signal Theory and Communications, University of Oviedo, Gijón, Spain, garciafmaria@uniovi.es

[2](Affiliation): Dept. of Signal Theory and Communications, University of Vigo, Vigo, Spain.

[3](Affiliation): Area of Signal Theory and Communications, University Rey Juan Carlos, Madrid, Spain.

***Abstract*—In this contribution, a methodology to process the measurements gathered with a novel subsurface imaging system is presented. This system is based on mounting a Ground Penetrating Radar (GPR) on board an Unmanned Aerial Vehicle (UAV). Among other advantages, the system does not need to be in contact with the soil, which is particularly useful for detecting dangerous objects (e.g., landmines). However, there are still several challenges that should be faced, such as speeding up the measurements processing so as to bring it closer to real-time operation. In this sense, two different focusing methods are applied to several in-flight measurements to generate a high-resolution synthetic aperture radar image by coherently combining all the measurements. This coherent combination is possible due to the use of a high accuracy positioning system. Both focusing methods are compared in terms of image quality and computational time for detecting metallic and dielectric targets.**

***Index Terms*—subsurface imaging, landmine detection, synthetic aperture radar, unmanned aerial vehicle.**

I. Introduction

In the last years, there has been a great development of Unmanned Aerial Vehicles (UAVs) for a wide range of new applications. Some of these applications, such as antenna measurement [1] and radar imaging [2], are based on mounting electromagnetic sensors. The advantages of UAV-based systems in terms of safety, measurement speed and inspection of difficult-to-access areas have fostered their usage in the field of security and defense (e.g., subsurface imaging for landmine detection).

Ground Penetrating Radar (GPR) has been widely used for subsurface sensing since it is able to provide images from the underground, thus enabling the detection of both metallic and dielectric targets [3]. There are mainly two different architectures of GPR systems: Forward-Looking GPR (FLGPR) [4] and Down-Looking GPR (DLGPR) [5]. In FLGPR the antennas are placed looking ahead of the vehicle, maximizing the penetration into the soil and reducing the reflections from the soil surface. However, it results in a lower resolution and thus, it is difficult to distinguish whether the targets are under or over the ground. In DLGPR the antennas are placed looking towards the soil. This provides a better resolution at the expense of worst penetration capabilities and stronger reflections from the soil surface.

In some applications, such as the aforementioned landmine detection, the detection system requires a standoff distance from the inspected area in order to minimize the risk. The first approach to keep this safety distance consists of using lightweight terrestrial robots. However, in order to reduce the risk even further and to increase the scanning speed, our approach is based on mounting a GPR on board a UAV [6]-[7], as shown in Fig. 1. Although some systems based on mounting a radar on board a UAV have been already presented, they have not been tested neither to detect buried targets (only targets on the surface) nor to create underground images [8]. On the other hand, our system has been already tested to detect both metallic and dielectric targets buried in a sandy soil. Furthermore, it has been shown that it can be used to obtain high resolution radar images using a Synthetic Aperture Radar (SAR) algorithm. Nevertheless, one of the remaining challenges is to speed up the measurements processing, working towards real-time imaging. This article is devoted to describe a methodology to process the measurements and to compare the performance and the results obtained with two different SAR algorithms (Delay-And-Sum, DAS, and Phase Shift Migration, PSM).

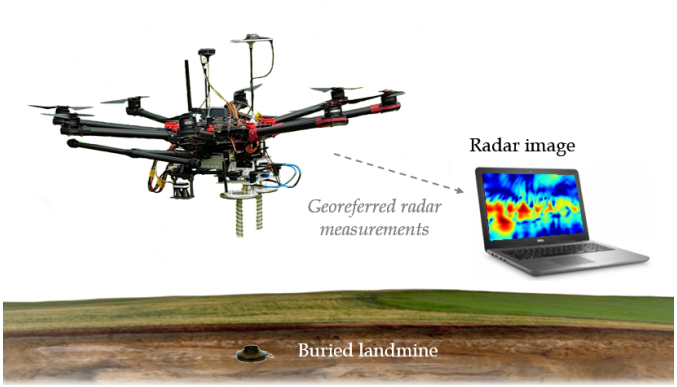

Fig. 1. Scheme of the proposed UAV-based GPR system for landmine detection.

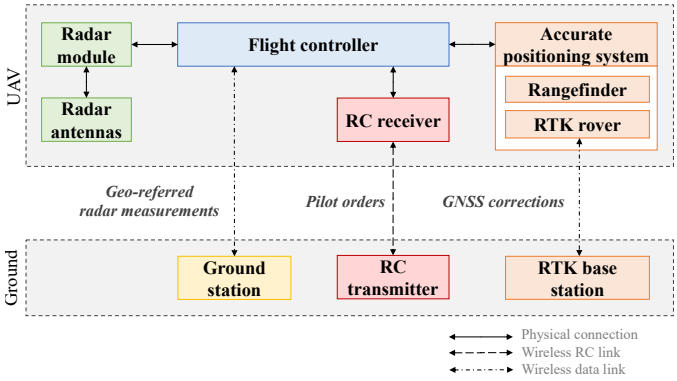

Fig. 2. Scheme of the main subsystems that compose the prototype.

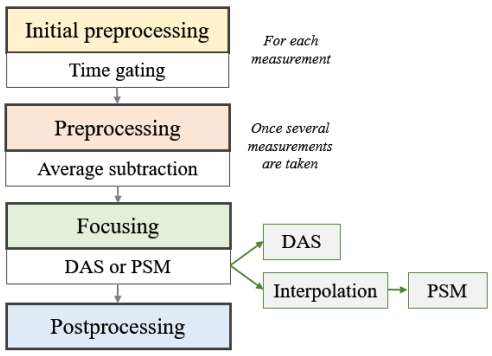

Fig. 3. Scheme of the methodology.

II. System Description

The proposed system is mainly based on mounting a GPR on board a UAV (as depicted in Fig. 1). The final goal is that the UAV autonomously flies over the inspected area, acquiring radar measurements which are georeferred and sent to a ground control station in real time. These measurements are processed to obtain images of the underground, thus enabling the detection of the possible buried targets.

The first prototype of the system is composed by the following subsystems (depicted in Fig. 2):

- Flight control subsystem, including a flight controller and positioning sensors usually on board conventional consumer UAVs (accelerometer, gyroscope, magnetometer, barometer and Global Navigation Satellite System - GNSS- receiver).
- Communication subsystem, which is composed by a radio control (RC) link at 433 MHz and a data link at 2.4 GHz.
- Accurate positioning subsystem, to achieve cm-level accuracy in order to enable the coherent combination of the radar measurements. It is composed by a Real Time Kinematic (RTK) system and a laser rangefinder to improve the height accuracy. RTK is a differential GNSS system that makes use of the carrier phase of the GNSS signals. It requires a static RTK base station, which transmits correction data to the RTK rover (on the UAV).
- Radar subsystem, which consists of a radar module and the radar antennas. This first prototype uses an impulse radar working at C-band (with 2 GHz bandwidth and 4 GHz center frequency) and two helix antennas with circular polarization and reverse handedness.
- Ground control station (e.g. a laptop), where the measurements are received and processed.

III. Methodology

In order to obtain high-resolution radar images, several measurements are taken along the inspected area, generating a synthetic aperture. It must be noticed that a point scatterer produces a hyperbolic or elliptical shape in the time-domain scan. Therefore, measurements must be coherently combined in order to obtain a well-focused image.

Furthermore, GPR is quite sensitive to the composition of the soil, the possible low contrast between the soil and the targets, and the soil surface roughness. In order to overcome these issues, additional signal processing techniques must be applied to the gathered data. Concerning the first issue, soil constitutive parameters can be estimated using datasheets or statistics from previous measurements [9]. If the soil constitutive parameters cannot be calculated and free-space propagation is assumed, the objects will be detected deeper than expected (due to the slower wave velocity in the soil) and the image will be worse focused. Regarding the other issues, the main challenge is to mitigate the strong clutter produced by the soil surface [10], which difficults the detection of the targets.

Taking into account all these considerations, the methodology to process the measurements collected with the prototype is structured as shown in Fig. 3. The main steps are:

- Initial preprocessing, which is applied to each measurement independently. In particular, in this contribution measurements are time gated to mitigate the coupling between the antennas.
- Preprocessing, which is performed once several measurements or after all measurements are gathered. In this case, it consists of subtracting the average signal from each measurement to partially remove the clutter. It may include other techniques, such as an algorithm to estimate the soil composition from the measurements.
- Focusing, where the measurements are coherently combined to obtain a SAR image.
- Postprocessing, which might include applying another clutter removal technique (such as a subspace projection method) and/or a feature extraction algorithm to the radar image.

In order to enhance the performance of the scanning system, real-time operation is desirable. In this sense, the focusing step is, in general, the most time-consuming stage in the methodology. As mentioned before, two different focusing strategies are compared in this contribution: DAS and PSM. This comparison is performed in terms of image quality and computational effort.

In the following subsections the equations of both methods are presented assuming a 2D scenario composed by two media,

with the interface between them placed at $z = z_0 < 0$. It is assumed that the scattered field E_{scatt} is measured on M acquisition points (placed at $\boldsymbol{r}_m$, with $m = 1, ..., M$) at N frequencies (f_n, with $n = 1, ..., N$) using a quasi-monostatic configuration (with the transmitter and receiver placed at almost the same position). Both algorithms can be straightforwardly extended to 3D scenarios.

A. Delay-And-Sum (DAS)

DAS basically consists of summing the radar measurements weighted by a phase correction term. This phase correction term takes into account the distance between the acquisition points $\boldsymbol{r}_m$ and the points where the reflectivity is computed [11].

The reflectivity at a single point $\boldsymbol{r'} = (x', z')$ is given by (1), where $\phi_n(\boldsymbol{r}_m, \boldsymbol{r}')$ is the phase shift corresponding to a wave propagating from $\boldsymbol{r}_m$ to $\boldsymbol{r}'$. This phase shift is computed using (2), where $k_{i,n}$ is the wave number in the $i-th$ medium at frequency f_n and $\boldsymbol{r}_i$ is the refraction point at the interface between the two media. According to the Snell's law, the calculation of this point requires solving a fourth order equation, which is numerically approximated using an iterative algorithm.

$$\rho(\boldsymbol{r}') = \sum_{m=1}^{M} \sum_{n=1}^{N} E_{\text{scatt}}(\boldsymbol{r}_m, f_n) e^{j2\phi_n(\boldsymbol{r}_m, \boldsymbol{r}')} \tag{1}$$

$$\phi_n(\boldsymbol{r}_m, \boldsymbol{r}') = \begin{cases} k_{0,n}\|\boldsymbol{r}_m - \boldsymbol{r}'\|, & z' \geq z_0 \\ k_{0,n}\|\boldsymbol{r}_m - \boldsymbol{r}_i\| + k_{1,n}\|\boldsymbol{r}_i - \boldsymbol{r}'\|, & z' < z_0 \end{cases} \tag{2}$$

It must be noticed that if the medium is homogeneous or if free-space propagation is assumed, then the phase-shift is given by the upper part of (2) for all z'.

B. Phase Shift Migration (PSM)

PSM is based on the exploding reflector concept, which has been initially used in seismic applications. This concept assumes that every reflection point explodes at time zero and, thus, only one-way propagation is considered.

PSM is derived from the scalar wave equation and it requires that the measurement points are uniformly distributed [12]. The reflectivity at a plane z' is given by (3), where $\mathcal{F}_x$ denotes the Fourier transform in the x domain, $E_{\text{scatt}}(k_x, f_n) = \mathcal{F}_x\{E_{\text{scatt}}(x, f_n)\}$ and $\varphi_n(z_m, z')$ is the phase-shift. This phase-shift is calculated according to (4), where $k_{z_{i,n}}$ is the z component of the wavenumber. $k_{z_{i,n}}$ is defined in (5), taking into account that in this formulation only one-way propagation is considered and thus, the wave velocity is half the true value.

$$\rho(z') = \mathcal{F}_x^{-1}\left\{\sum_{n=1}^{N} E_{\text{scatt}}(k_x, f_n) e^{j\varphi_n(z_m, z')}\right\} \tag{3}$$

$$\varphi_n(z_m, z') = \begin{cases} k_{z_{0,n}}(z_m - z'), & z' \geq z_0 \\ k_{z_{0,n}}(z_m - z_0) + k_{z_{1,n}}(z_0 - z'), & z' < z_0 \end{cases} \tag{4}$$

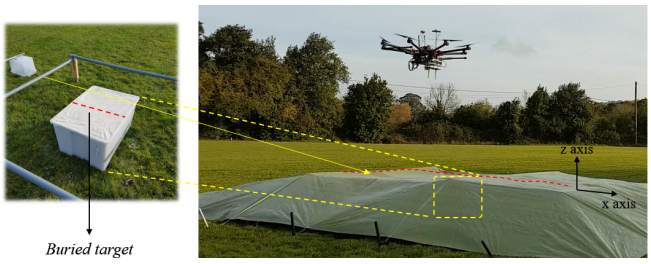

Fig. 4. Setup for the in-flight tests.

$$k_{z_{i,n}} = \sqrt{4k_{i,n}^2 - k_x^2} \tag{5}$$

As explained for the DAS algorithm, if a homogeneous medium is assumed, the phase-shift is given by the upper part of (4).

Due to the irregular movement of UAVs, it is not possible to acquire uniformly distributed measurements with the UAV-mounted radar. Thus, measurements are interpolated into a uniform grid before processing them with PSM.

IV. Results

The validation of the proposed UAV-based GPR system has been carried out in several stages, from measurements in the laboratory to in-flight tests with the prototype. Since it is not possible to dig in the airfield, a plastic box filled with sand has been used to bury the targets for the flight tests. The box, which has a size of (56, 78, 43) cm^3, was placed over the grass of the airfield. It was covered with a canvas supported by a PVC structure so as to simulate a smoother surface, as shown in Fig. 4.

Measurements with both metallic and dielectric targets are presented in this contribution. As explained in the previous section, time-gating and average subtraction are applied before the focusing step to mitigate the clutter and the coupling between the antennas. Since measurements are taken using an impulse radar, a Fourier Transform is applied before the focusing algorithm. Furthermore, it must be remarked that, in order to obtain a good interpolation for the PSM method, the UAV is programmed to maintain a steady altitude.

A. Detection of a metallic target

A metallic disk of 9-cm radius and 1-cm thickness was buried at 12-cm depth. Assuming free-space propagation, the SAR image for the whole aperture (of 2.5 m size) is shown in Fig. 5 for both DAS and PSM algorithms. In both cases, the air-sand interface and the buried target are clearly detected. Furthermore, the air-grass interface, the PVC bars that support the canvas and even the sand-grass interface (below the sandbox) are also distinguishable. It must be noticed that the buried target and the sand-grass interface are detected deeper than expected since the sand permittivity has not been taken into account. Comparing DAS and PSM results, it can be concluded that DAS seems to be more affected by positioning errors, yielding a noisier image than PSM.

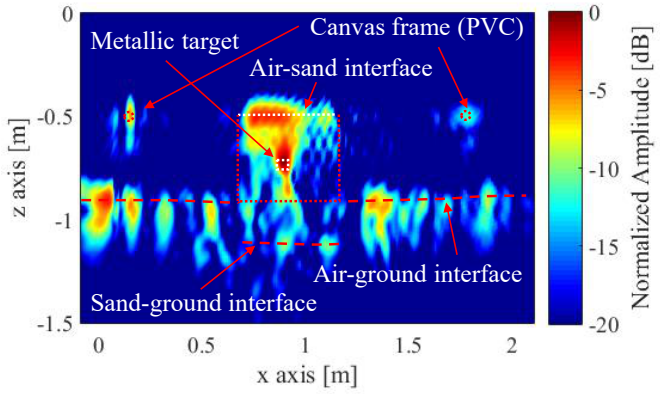

(a) DAS

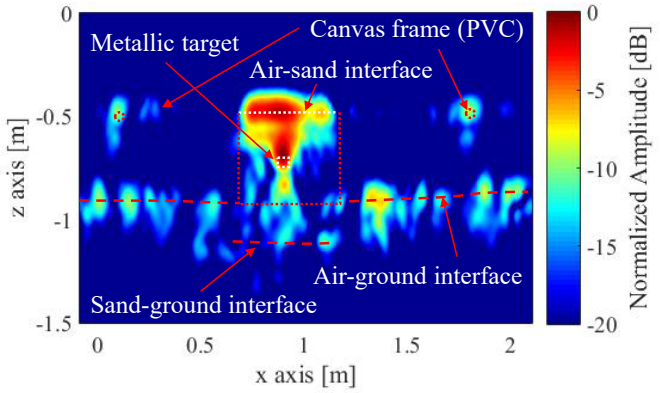

(b) PSM

Fig. 5. Imaging results (with a metallic target) for the whole aperture assuming free-space propagation.

Then, the aperture was restricted to a 60-cm length over the sandbox. In this case, the material characteristics of the two-layer scenario have been considered, being the first layer air ($\varepsilon_{r,0} = 1$) and the second one dry sand ($\varepsilon_{r,1} \approx 2.5$) [9]. The resulting images are shown in Fig. 6, where both the target and the sand-grass interface are detected at their true depth. Since the aperture length is smaller, the cumulative positioning error is also smaller. Therefore, the results of DAS are less noisier than for the larger aperture and they are also more similar to those obtained with PSM. The reduction of the aperture length also yields to a lower cross-range resolution, which is partially compensated with the smaller cumulative positioning error.

B. Detection of a non-metallic target

A plastic cylinder with 9-cm radius and 9.5-cm height (filled with foam) was buried in the sand box at 10-cm depth. Considering free-space propagation, the SAR images obtained with both methods for the whole aperture are shown in Fig. 7. They are similar to those obtained with the metallic target. The main differences are the target size, which is bigger in this case, and the sand-grass interface, which is slightly better detected.

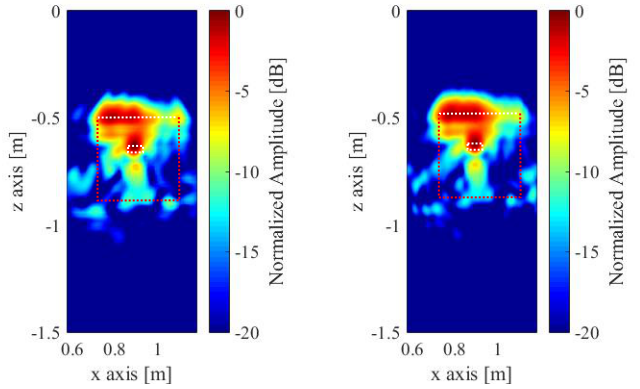

(a) DAS (b) PSM

Fig. 6. Imaging results (with a metallic target) for the sand-box area taking into account the soil composition.

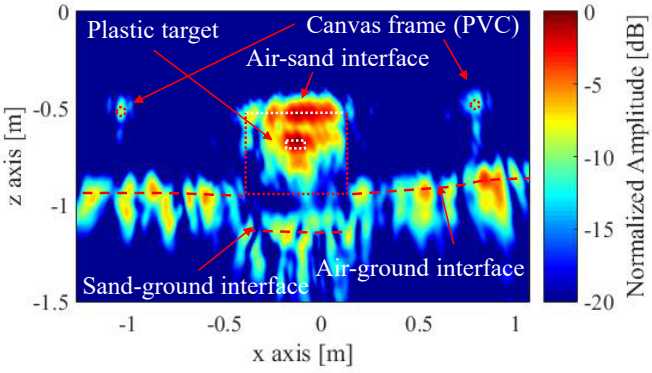

(a) DAS

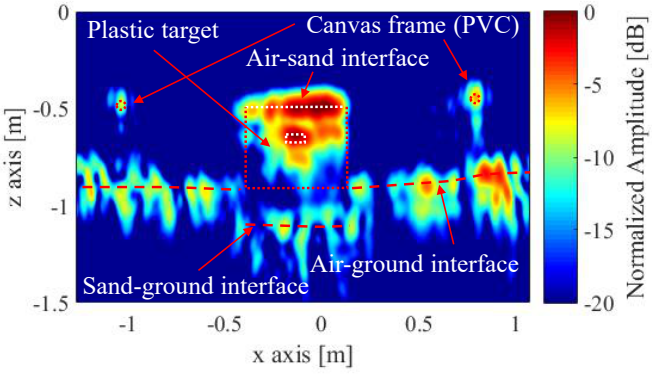

(b) PSM

Fig. 7. Imaging results (with a non-metallic target) for the whole aperture assuming free-space propagation.

The aperture was then restricted to a 60-cm length over the sandbox. As in the previous subsection, the same two-layer scenario has been considered. The SAR images are shown in Fig. 8, where the target is detected at its true depth. In addition, since the target is not metallic, the reflection coming from the sand-grass interface is more noticeable.

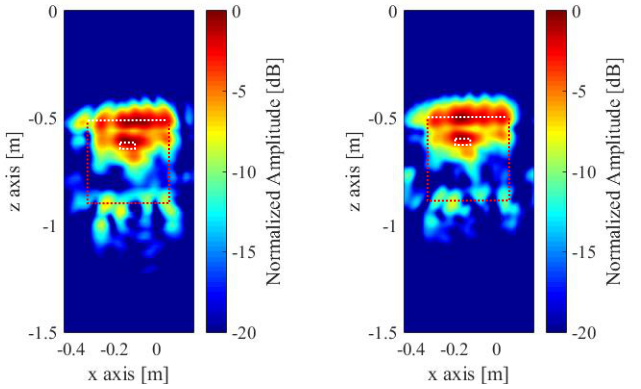

(a) DAS (b) PSM

Fig. 8. Imaging results (with a non-metallic target) for the sand-box area taking into account the soil composition.

TABLE I
COMPARISON OF COMPUTATIONAL TIMES FOR DIFFERENT APERTURE LENGTHS (L_{ap}).

L_{ap} [m]	DAS-1L [s]	DAS-2L [s]	PSM-1L [s]	PSM-2L [s]
2	2.4	10.6	0.45	0.45
1	0.6	3.0	0.21	0.22
0.6	0.3	1.0	0.15	0.16

C. Comparison of computational time

Once the results of DAS and PSM have been compared qualitatively, this subsection is devoted to analyze their computational performance. Table I shows the computational time of each method for several aperture lengths and for scenarios assumed to be composed by one and two layers of different materials (denoted as 1L and 2L, respectively). Both algorithms have been run in a conventional laptop (with i7-4700HQ processor and 16 GB of RAM) without parallelization. Since PSM is mainly based on using FFTs (Fast Fourier Transforms), it is clearly faster than DAS. This difference is especially more significant when considering a two layer scenario. Furthermore, it must be noticed that the main time consuming operation in PSM is the interpolation, which must be performed as initial task.

V. CONCLUSION

In this contribution, a methodology to process measurements taken with a UAV-based GPR system has been presented. The main advantages of the system are related to scanning speed, security and cost. In addition, thanks to the use of a high accuracy positioning system, measurements can be coherently combined using a focusing algorithm, which provides a high-resolution SAR image. Two focusing strategies (DAS and PSM) have been compared to detect both metallic and non-metallic targets with in-flight measurements. PSM seems to be less affected by positioning errors, providing cleaner images than DAS. Furthermore, since PSM is based on FFTs, it is notably faster than DAS.

ACKNOWLEDGMENT

This work has been partially supported by Government of Spain (under projects TEC2014-54005-P, TEC2015-73908-JIN and TEC2014-55290-JIN, and grant FPU15/06341), Government of Asturias (under projects IDI/2017/000095 and GRUPIN-18-000191), Government of Galicia and AtlantTIC.

REFERENCES

[1] M. Garcia-Fernandez, Y. Alvarez-Lopez, and F. Las Heras, "On the use of Unmanned Aerial Vehicles for antenna and coverage diagnostics in mobile networks," *IEEE Communications Magazine*, vol. 56, no. 7, 2018.

[2] M. Llort, A. Aguasca, C. Lopez-Martinez, and T. Martinez-Marin, "Initial evaluation of SAR capabilities in UAV multicopter platforms," *IEEE Journal of Selected Topics on Applied Earth Observation and Remote Sensing*, Vol. 11, No. 1, pp. 127-140, 2018.

[3] D. J. Daniels, *Ground Penetrating Radar,, 2nd ed.* London: IET, 2004.

[4] G. Liu, Y. Wang, J. Li, and M. R. Bradley, "SAR imaging for a forward-looking GPR system," in *AeroSense 2003*, pp. 322333, 2003.

[5] E. M. Rosen, and E. Ayers, "Assessment of down-looking GPR sensors for landmine detection," in *Proc. SPIE 5794, Detection and Remediation Technologies for Mines and Minelike Targets X*, pp. 423434, 2005.

[6] B. Gonzalez, Y. Alvarez, A. Arboleya, Y. Rodriguez, M. Garcia-Fernandez, F. Las Heras, and A. Pino, "Airborne systems and detection methods for the localization and production of images of buried objects and characterization of the subsurface composition," ES Patent 2577403, 2016.

[7] M. Garcia-Fernandez, Y. Alvarez-Lopez, A. Arboleya-Arboleya, B. Gonzalez-Valdes, Y. Rodriguez-Vaqueiro, F. Las Heras, and A. Pino, "Synthetic Aperture Radar imaging system for landmine detection using a Ground Penetrating Radar on board an Unmanned Aerial Vehicle," *IEEE Access*, vol. 6, 2018.

[8] G. Ludeno, I. Catapano, G. Gennarelli, F. Soldovieri, A. Vetrella, A. Renga, and G. Fasano, "A micro UAV borne system for radar imaging: a feasibility study," in *9th International Workshop on Advanced Ground Penetrating Radar*, Edinburgh, 2017.

[9] A. Martinez, and A. P. Byrnes. "Modeling Dielectric-Constant Values of Geologic Materials: An Aid to Ground-Penetrating Radar Data Collection and Interpretation," *Current Research in Earth Sciences*, bulletin 247, part 1, 2001.

[10] R. Solimene, A. Cuccaro, A. DellAversano, I. Catapano, and F. Soldovieri, "Ground clutter removal in gpr surveys," *IEEE Journal of Selected Topics in Applied Earth Observations and Remote Sensing*, vol. 7, pp. 792798, 2014.

[11] J. A. Martinez-Lorenzo, C. M. Rappaport, and F. Quivira, "Physical limitations on detecting tunnels using underground-focusing spotlight synthetic aperture radar," *IEEE Transactions on Geoscience and Remote Sensing*, vol. 49, pp. 6570, 2011.

[12] M. Fallahpour, J. T. Case, M. T. Ghasr, and R. Zoughi, "Piecewise and wiener filter-based SAR techniques for monostatic microwave imaging of layered structures," *IEEE Transactions on Antennas and Propagation*, vol. 62, pp. 282294, 2014.